

Article

## Coupled Wave Energy and Erosion Dynamics along a Salt Marsh Boundary, Hog Island Bay, Virginia, USA

Anthony M. Priestas <sup>1,2</sup>, Giulio Mariotti <sup>1,3</sup>, Nicoletta Leonardi <sup>1</sup> and Sergio Fagherazzi <sup>1,\*</sup>

<sup>1</sup> Department of Earth and Environment, Boston University, 675 Commonwealth Ave Boston, MA 02215, USA; E-Mails: anthony.m.priestas@usace.army.mil (A.M.P.);

gmariotti@lsu.edu (G.M.); nicleona@bu.edu (N.L.);

<sup>2</sup> United States Army Engineer Research and Development Center, Coastal and Hydraulic Laboratory, 3909 Halls Ferry Road, Vicksburg, MI 39180, USA

<sup>3</sup> Department of Oceanography and Coastal Sciences, Louisiana State University, 1002-Q EC&E Building, Baton Rouge, LA 70803, USA

\* Author to whom correspondence should be addressed; E-Mail: sergio@bu.edu; Tel.: +1-617-353-2092.

Academic Editor: Charitha Pattiaratchi

Received: 1 July 2015 / Accepted: 9 September 2015 / Published: 15 September 2015

---

**Abstract:** The relationship between lateral erosion of salt marshes and wind waves is studied in Hog Island Bay, Virginia USA, with high-resolution field measurements and aerial photographs. Marsh retreat is compared to wave climate calculated in the bay using the spectral wave-model Simulating Waves Nearshore (SWAN). We confirm the existence of a linear relationship between long-term salt marsh erosion and wave energy, and show that wave power can serve as a good proxy for average salt-marsh erosion rates. At each site, erosion rates are consistent across several temporal scales, ranging from months to decades, and are strongly related to wave power. On the contrary, erosion rates vary in space and weakly depend on the spatial distribution of wave energy. We ascribe this variability to spatial variations in geotechnical, biological, and morphological marsh attributes. Our detailed field measurements indicate that at a small spatial scale (tens of meters), a positive feedback between salt marsh geometry and wave action causes erosion rates to increase with boundary sinuosity. However, at the scale of the entire marsh boundary (hundreds of meters), this relationship is reversed: those sites that are more

rapidly eroding have a marsh boundary which is significantly smoother than the marsh boundary of sheltered and slowly eroding marshes.

**Keywords:** salt-marsh erosion; wind-waves; wave modeling

---

## 1. Introduction

Salt marshes are among the most productive ecosystems on Earth and provide a variety of ecosystem services, such as storm protection of coastal cities, nutrients removal, and carbon storage [1–3]. In spite of their important services, salt marshes are continuously threatened by external forcing such as wave action, sea-level rise, decrease in sediment supply, and land reclamation. As a result, large salt marsh losses have been documented worldwide [4–8]. Understanding salt marsh dynamics and morphological evolution is, thus, a key issue for society and a critical component for the correct management and preservation of these coastal wetlands.

Salt marshes have been found to be able to keep pace with sea-level rise and to be inherently stable along the vertical direction due to feedbacks between inundation, organic matter production, and vertical accretion [9,10]. On the contrary, they appear unstable along the horizontal direction and weak with respect to the action of wind waves due to the lack of feedbacks between processes leading to lateral erosion and those contributing to salt marsh expansion [11,12]. Marsh erosion due to wind-waves attack has long been recognized as a mechanism for marsh loss and many studies have focused on the qualitative description of edge erosion and mechanics, and/or quantifying erosion rates through time [13–21].

The rate of erosion depends on several parameters, such as soil type, marsh platform elevation, vegetation, and macrofauna. For instance, Leonardi and Fagherazzi [5,6] showed that the presence of a local variability in soil resistance affects the shape of marsh boundaries and the large-scale morphodynamic response of salt marshes to wind waves. A field study in Galveston Bay, Texas, indicated that sites with clay soils eroded less than those with loamy soils [15]. This is in agreement with wave-tank experiments conducted by Feagin *et al.* [22], in which they showed that marsh soils with higher sand content are more erodible, and found that one of the main mechanisms by which vegetation prevents erosion is by modifying soil parameters. Macrofauna can also affect the resistance of marsh boundaries. Vegetation grazing by crabs can trigger vegetation die-off on marsh banks reducing the overall bank stability [23]. Burrowing by crabs also facilitates sediment removal and localized erosion [24]. In some instances, lateral erosion of salt marshes has been directly linked to infestation by burrowing crustaceans [25].

Hall *et al.* [15] also found that the passage of Hurricane Alicia (which made landfall 80 km from their study site) did very little to accelerate erosion, and concluded that high water levels brought by the storm surge protected the shoreline from edge erosion. This process was confirmed by Tonelli *et al.* [26] who demonstrated, using a high-resolution Boussinesq model, that wave forcing at marsh edges increases with water level up to the point when the marsh is submerged, and then it rapidly decreases. Therefore, boundary erosion primarily occurs in period of storminess when water level is around mean sea level and close to the marsh platform elevation.

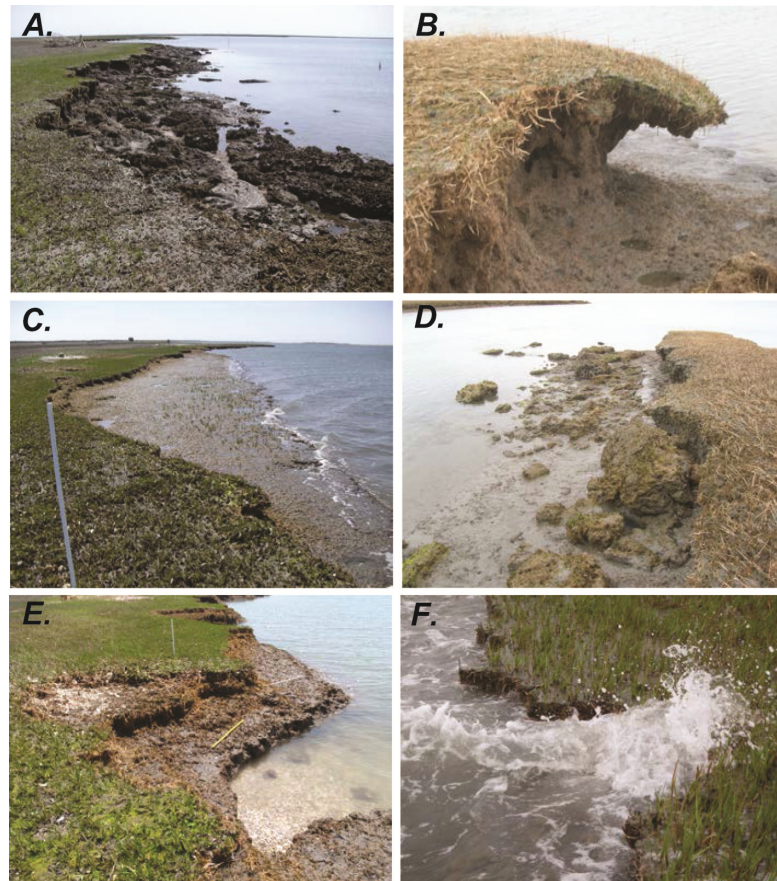


**Figure 1.** Degradation of marsh scarps in Hog Island Bay, Virginia. The action of waves at lower water levels can remove previously eroded material (**A**) and cause undercutting (**B**); The process of root scalping occurs when waves attack the marsh at water levels approaching the marsh platform elevation (**C**); toppling is also common (**D**); Examples of wave gully: at low tide (**E**) and during a storm with wave energy concentration (**F**).

The erosion of salt marshes by wind waves can follow different styles, such as undercutting of the marsh scarp and consequent cantilever failure (Figure 1B,D), as also reported by Allen [19]. Waves tend to break offshore at low tide while also being small due to the limited water depth, which can result in a local lowering of the intertidal basin by removing previously eroded material (Figure 1A). Wave-cut gullies [27] are sub-triangular features that incise the marsh shoreline due to wave impact along scarped edges made of cohesive soils (Figure 1E,F). These features were previously noted in the literature as “points” and “cuts” by Hall *et al.* [15] and “clefts” and “necks” by Schwimmer [28]. Analysis of the hydrodynamics within a 10 m gully along the Louisiana coast revealed that run-up velocities increase at the gully head as a result of wave-crest compression owing to the gully’s convergent geometry [27]. Because of the increased energy by wave concentration, erosion at the gully head is often three to five times greater than that at the shoreline [27]. When waves occur at water elevations near that of the marsh platform, they may strike against the weak boundary separating the live vegetation root layer from the peat layer, which occurs at about 20 cm depth. The upward force of the impinging waves was observed in the field to torque the root mat upward, which results in uprooting and removal of the active root layer, a process termed “root-scalping” (Figure 1C). Marsh

boundary erosion can also be caused by crabs that excavate burrows in the vegetation substrate, thus, removing material and weakening the bank [24,25].

Despite the number of processes that can modify marsh boundary erosion and dynamics, we maintain that direct wave attack is the major driver of erosion in marshes fringing open bays. Therefore, we focus primarily on quantifying the relationship between shoreline retreat, wave energy, and shoreline geometry. Specifically, the goal of this paper is three-fold: (1) to review existing formulations linking salt-marsh erosion to wave power; (2) to investigate the relationship between erosion rates and marsh shoreline geometry; and (3) to quantify seven-year erosion rates as a function of wind-induced wave power and water level.

Our analysis is based on high-resolution data collected at the Virginia Coast Reserve, USA. At this site, McLoughlin *et al.* [7] compared rates of shoreline change determined by aerial photographs between 1957 and 2007 with wave data calculated with the numerical model Simulating WAVes Nearshore (SWAN). McLoughlin *et al.* [7] found a relationship between wave energy flux and volumetric erosion rates along the marsh edges. Herein we extend the analysis of McLoughlin *et al.* [7] to a much higher spatial (field measurements of erosion at the sub-meter scale) and temporal resolution (monthly to yearly intervals). We further expand the analysis to the entire bay boundary (33 sites *versus* the three sites of McLoughlin *et al.* [7]).

**2. Review of Existing Formulations for Wave Erosion of Marsh Boundaries**

Schwimmer [28] quantified marsh boundary retreat rates over a five-year period along sites within Rehoboth Bay, Delaware, USA. Wind, bathymetric, and fetch data were used to hindcast the wave climate from which the total averaged wave power at each site was computed. Based on these data, Schwimmer [28] derived an empirical time-averaged erosion rate, *R* (m/year), as function of wave power, *P* (kW per meter of shoreline) expressed as:

$$R = 0.35P^{1.1} \tag{1}$$

Mariotti *et al.* [29] showed that wave energy impacting the marsh shoreline is sensitive to changes in wind direction and sea-level rise since a deeper tidal basin would result in greater wave energy. Additionally, Mariotti and Fagherazzi [30] modeled the 1-D evolution of a scarped marsh boundary in which the erosion rate, *R*, was expressed as:

$$R = \beta(P - P_{cr}) \tag{2}$$

where  $\beta$  is a constant, *P* is the average wave power, *P<sub>cr</sub>* is a critical threshold below which no erosion occurs. In this case, however, the equation was only used to determine the morphodynamics of the marsh scarp considering waves, tides, sediments, and vegetation, and was not empirically derived; therefore, it has not been tested against field data and may lack predictive power.

Marani *et al.* [31] derived a theoretically based equation for boundary retreat using Buckingham’s theorem of dimensional analysis with five parameters. In this way, they expressed the erosion process as two non-dimensional groups for which they derived the relationship:

$$\frac{Rhc}{P} = f\left(\frac{h}{d}\right) \tag{3}$$

where  $R$  is the erosion rate,  $h$  is the scarp height (with respect to the tidal flat),  $c$  is a sediment cohesion factor,  $P$  is the mean power density of the waves,  $d$  is the water depth (with respect to mean sea level), and  $f$  is a function later found to be nearly constant. Therefore, the volumetric erosion rate was expressed as a linear function of mean wave power in contrast to the power law of Schwimmer [28]:

$$V = \alpha P \quad \text{with} \quad V = Rc \tag{4}$$

where  $\alpha$  is a constant of proportionality. By determining the erosion rates along 150 sites of the Venice Lagoon using historical aerial imagery, Marani *et al.* [31] determined the average volumetric erosion rate ( $\text{m}^2 \cdot \text{year}^{-1}$ ) for the marshes as:

$$V = 0.03P + 0.19 \tag{5}$$

The slope of the relation, and therefore the rate of erosion, likely depends on soil type, water elevation, and possibly other factors, such as vegetation and macrofauna. Leonardi and Fagherazzi [5,6] used the formulation:

$$E_i = \alpha P^\beta \exp\left(-\frac{H_{ci}}{H}\right) \tag{6}$$

where  $\alpha$ , and  $\beta$  are constant coefficients [28],  $P$  is the wave power, and  $H$  is the wave height. The subscript  $i$  refers to salt marsh portions which are homogeneous in terms of marsh platform erosional resistance,  $E_i$  is the erosion rate of the above mentioned homogeneous marsh portions,  $H_{ci}$  is the critical height for marsh boundary stability and can be calculated from soil shear strength values [32]. This formulation has been found in agreement with long-term field data of marsh boundary erosion and soil shear strength at five sites along the United States Atlantic Coast. The formula allows taking into account variability in erosional resistance along the marsh platform due to biological and ecological processes, and is suitable to reproduce the frequency-magnitude distribution of erosion events, as well as complex marsh boundary morphological features [5,6]. The formulation is such that when wave forces are very high ( $H \gg H_{ci}$ ), the exponential goes to one, and every marsh portion looks the same in front of the main external driver with the same erosion probability. On the contrary, when wave energy is very low ( $H \leq H_{ci}$ ), variability in erosional resistance is more important and weakest elements are easily eroded. According to this formulation, different values of marsh boundary sinuosity have been related to different wind wave exposures. Specifically, high wave-power values cause more uniform marsh boundary profiles. On the contrary, salt marshes exposed to low wave-power conditions, and slowly eroding marshes, have been found to display rougher marsh boundary profiles [5,6]. Moreover, while rapidly eroding salt marshes display a Gaussian frequency-magnitude distribution of erosion events, slowly eroding salt marshes have been found to be characterized by long tailed frequency-magnitude distribution with a large number of small erosion events and a few number of unpredictable and high magnitude episodes.

Salt marsh lateral retreat has been also related to wave thrust values at the marsh boundary [26]. Wave thrust is defined as the integral along the vertical of the dynamic pressure of waves. It has been shown that wave thrust is highly dependent on tidal levels. Specifically, wave thrust increases with tidal elevations until the marsh is submerged, and at that point the wave thrust starts to rapidly

decrease. Decreasing wave thrust is attributed to wave breaking and wave energy dissipation on the vegetated marsh platform.

Herein, we will further test the relationship between wind-wave exposure and salt-marsh lateral retreat. We correlate salt-marsh lateral retreat with both wave power and wave thrust values at corresponding locations. The existence of a relationship between wave forcing and salt-marsh lateral retreat has been verified for cumulative values of the mentioned variables, as well as for their annual averages. Cumulative values are cumulative erosion (m), and cumulative wave energy (MJ/m) relative to time spans between field surveys.

### 3. Study Area

The study area is part of the Virginia Coast Reserve Long-Term Ecological Research network (VCR-LTER), which comprises a 110-km dynamic system of barrier islands, shallow lagoons, and salt marshes separated by deep tidal inlets. Our research is focused within Hog Island Bay, a coastal barrier lagoon located along the Atlantic side of the southern Delmarva Peninsula (Figure 2). The lagoon is roughly 150 km<sup>2</sup> of predominately open water and is characterized by intertidal and subtidal basins with mainland fringe-marshes to the west, backbarrier-fringe marshes to the east, and platform marshes to the north and south. Vegetation on the salt marshes is dominated by short-form *Spartina alterniflora* with an average stem height of 30 cm. The majority of the marshes have a prominent scarp at their seaward edges, which are typically 1.0–1.5 m above the elevations of the adjacent tidal flats.

The average water depth for most of the lagoon is about 2 m with respect to mean low water (MLW) and rarely exceeds 3 m [33]. Semidiurnal tides have a mean tidal range of about 1.2 m (NOAA station 8631044). Water exchange occurs primarily through the Great Machipongo Inlet, maintained by a submerged deep thalweg that spans the lagoon floor to the mainland [33].

Local weather patterns are dominated by the Bermuda high-pressure system [34], giving rise to mostly calm conditions in the lagoon during the summer months, and the passage of cold fronts and Northeasters during winter [35], which are largely responsible for storm conditions, in addition to occasional hurricanes. The area is highly influenced by storm disturbances, receiving an average of 20 extratropical storms per year [36]. The distribution of wind speed and direction measured from 1993 to 1996 reveals that the most frequent wind directions originate between 180°–210° N and 330°–60° N with wind speeds usually less than 12 m/s [29].

## 4. Methods

### 4.1. Field Survey of Marsh Shoreline Erosion

Three marsh sites (Matulakin Marsh, MM, Chimney Pole, CP, and Hog Island, HI) were selected in order to encompass different shoreline positions and orientations (white stars in Figure 2). Retreat rates and morphology of the marsh shorelines were monitored through repeated surveys over a time span of three years from August 2007 to April 2010 (Figure 3). Shoreline positions were measured using a Topcon laser-surveying total station. The time-spans between successive surveys are the following: 29 days, 6 May 2008 to 6 June 2008; 77 days, 6 June 2008 to 21 August 2008; 202 days, 21 August 2008 to 11 March 2009; 397 days, 11 March 2009 to 13 April 2010.



**Figure 2.** Marshes in Hog Island Bay, part of the Virginia Coast Reserve, Virginia, USA. HI is Hog Island Marsh; CP is Chimney Pole Marsh, MM is Matulakin Marsh. Central Bay (CB) is the position where a wave gauge was deployed. White segments indicate marsh boundaries where erosion rates were measured with aerial images.

At each site, direct measurements of edge erosion were also made by using 6–7 erosion pins inserted horizontally into the marsh scarp. Due to the exploratory nature of field observations at the beginning of this research, the start times differ somewhat between sites. The total durations of erosion pin measurements at each site are as follows: MM (824 days, 9 January 2008 to 13 April 2010), CP (959 days, 28 August 2007 to 13 April 2010), HI (959 days, 28 August 2007 to 13 April 2010). Pins were reset after each measurement unless eroded out, in which case they were replaced.

Shoreline surveys yielded three pieces of information: (1) estimation of erosion rates along the length of the boundary; (2) characterization of shoreline morphology changes; and (3) computation of the frequency-magnitude distribution of erosion events and shoreline sinuosity to be related to wind wave exposure.

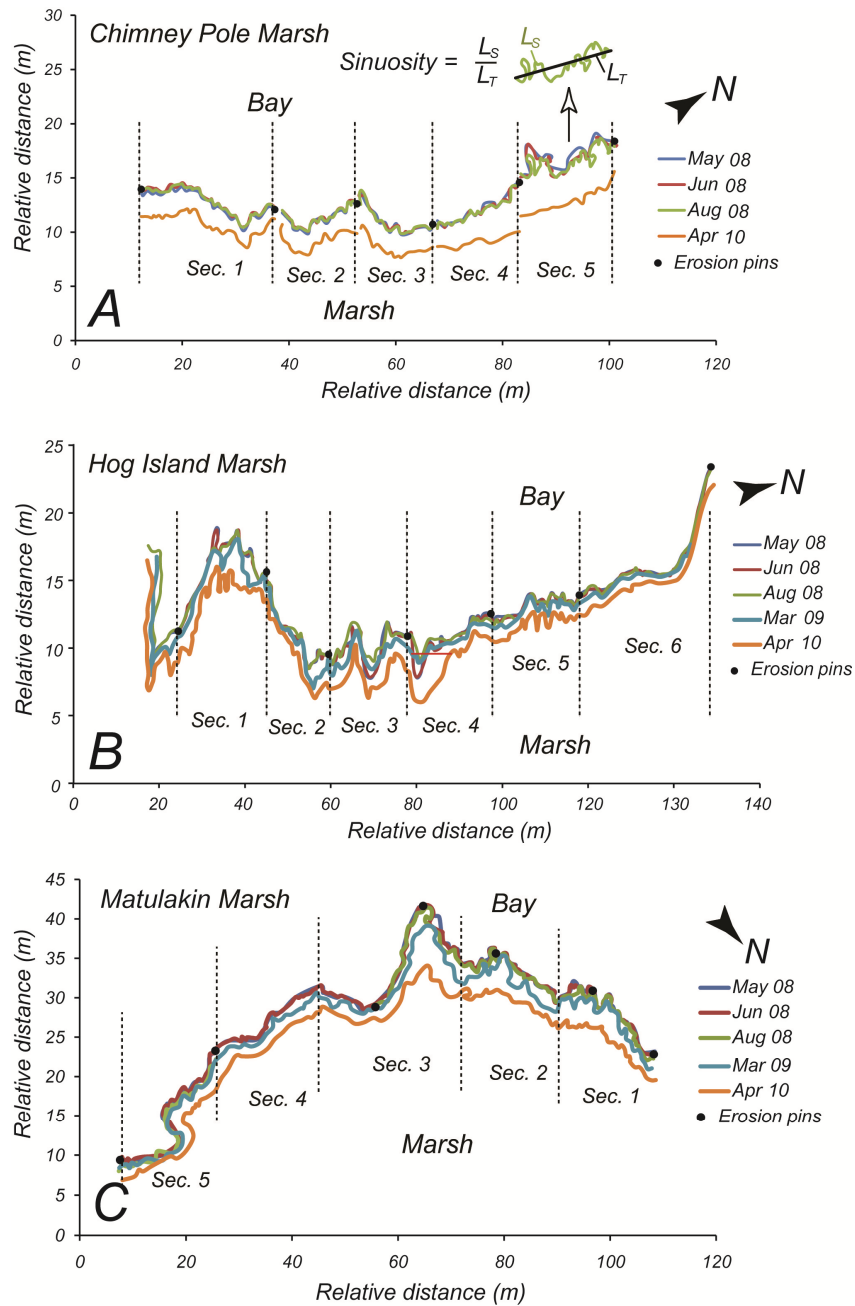


**Figure 3.** High resolution surveys of marsh boundaries in Hog Island Bay between 2008 and 2010. **(A)** Chimney Pole Marsh; **(B)** Hog Island Marsh; **(C)** Matulakin Marsh. The vertical scale is distorted to better appreciate variations in boundary sinuosity. An example of boundary sinuosity calculation is reported in **(A)**.

Marsh boundary sinuosity for the three sites has been calculated at two different scales: at the scale of the entire boundary length (order of hundreds of meters), and at a smaller scale (order of tens of meters). We maintain that at the scale of the entire marsh boundary length, variability in erosional resistance is present and there are thus stretches of marsh boundary that are more susceptible to erosion than others. This is due to the variety of biological and ecological mechanisms acting along marsh boundaries. On the contrary, we assume that at smaller scale (tens of meters), corresponding stretches of shoreline are relatively uniform in terms of erosional resistance, while also being sufficiently long to allow reasonable sinuosity calculations.

When calculating the marsh boundary sinuosity at a smaller scale our goal is to separate the influence of variability in erosional resistance along the marsh boundary [5,6] from the influence of wind waves on marsh boundary sinuosity, and focus on the latter. Sinuosity values were calculated as the ratio between boundary length and the length of the straight line between the two marsh boundary end points (Figure 3A). Comparison in time between the same stretches of shoreline (Figure 3) was used to evaluate the erosion rate between measuring periods.

Measurements of marsh boundary retreat with erosion pins and boundary surveys have limitations which need to be taken into account. For example, erosion pin measurements only provide few data points as representative of the entire marsh boundary. Regarding the surveys, the edge of the marsh scarp was not always well defined and it was assumed that the vegetation front would demarcate the boundary (we thus followed the definition of marsh as vegetated surface). In this situation, erosion rates determined from surveys would sometimes overestimate the total volume of sediment removed, since the root mat of the vegetation can recede faster than the scarp itself at some locations.

#### 4.2. Estimating Marsh Erosion from Aerial Photographs

Field measurements of marsh shoreline erosion have limitations connected to the fact that they are only feasible for relatively small spatial extents. To overcome this limitation, we further determined erosion rates at 33 locations around the lagoon using two ortho-images from 2002 and 2009 (Figure 2, continuous white lines). The aerial image from 2002 is part of the Virginia Geographic Information Network (VGIN), is available for public download by the GIS Center at Radford University, and was produced by VARGIS LLC of Herndon, Virginia. The acquisition date over the study area was 19 January 2002, the image was developed at a resolution of 2 m (1:400), and referenced in Virginia (south) state plane coordinate system.

The digital orthophotograph from 2009 is part of the National Agriculture Imagery Program (NAIP) and is available through the Aerial Photography Field Office (APFO) of the USDA Farm Service Agency. These images were acquired at a resolution of 1 m (1:200) and were rectified within  $\pm 6$  m to true ground before being published. The images were then referenced to UTM zone 18 coordinate system using the North American Datum of 1983 (NAD 83). The 2002 and 2009 aerial images for the region were added into ArcMap using APFO's ArcGIS server, and were then georeferenced in ArcMap to the 2009 imagery.

#### 4.3. Modeling Wind Waves and Determination of Wave Power

##### 4.3.1. Wave Hindcasting

Wave regime in the VCR lagoons was hindcasted using the spectral wave model SWAN, which solves the transport equations for wave action density, and accounts for shoaling, refraction, wind waves generation, wave breaking, bottom dissipation, and non-linear wave interactions [37–39]. A rectangular grid with 200 by 300 cells with a resolution of 150 m was used to represent the lagoons' bathymetry (Figure 4). For the wind term, the exponential wind input of Yan [40] and the linear growth of Cavaleri and Malanotte-Rizzoli [41] were used in the simulations. The process of whitecapping was represented by the van der Westhuysen *et al.* [42] formulation, based on the azimuthal-integrated

spectral saturation. Depth induced breaking was described by the physically-based formulation of van der Westhuysen *et al.* [43], which relates the nonlinearity of breaking waves in shallow water to wave asymmetry.

A total of 900 simulations were performed, combining 15 water levels (every 0.2 m, from -0.8 m below M.S.L. to 2 m above M.S.L.), 5 wind speeds (5, 10, 15, 20, 25 m/s) and 12 wind directions (every 30°). In each simulation, water level, wind speed, and direction were imposed uniform throughout the domain. Simulations were performed in steady conditions, *i.e.*, the wave field was in local equilibrium with the energy sink-source terms. We also assumed that the wave direction is always corresponding to the wind direction, given the small fetch and the absence of waves propagating from offshore. For each simulation, a single value of the significant wave height,  $H$ , and peak wave period,  $T$ , were extracted at each marsh boundary position,  $i$ . We therefore obtained two discrete functional relationships, relating  $H$  and  $T$  to the water level,  $y$ , wind speed,  $U$ , and direction,  $\alpha$ , at each marsh boundary position:

$$H_i = f_1(y, U, \alpha, i); T_i = f_2(y, U, \alpha, i) \quad (7)$$

The relationship between  $H_i$  and  $T_i$  was made continuous through a linear interpolation.

Water-level measurements were retrieved from the Wachapreague NOAA station (ID 8631044). Lawson *et al.* [44] modeled waves in Hog Island Bay with SWAN using the wind speed from the Kiptopeke NOAA station (ID KPTV2), whose record started in 2005. In order to base our results on a longer time series, we instead use the wind speed and direction data from the NOAA station CHLV2-Chesapeake Light, whose record started in 1984. This station is located outside the lagoons, about 10 km from the coastline, and likely overestimates the wind speed within the lagoons.

After comparison, we determined that the wind speed from the Chesapeake Light station is 20% higher than the wind speed at the Kiptopeke station when data are available at both stations, while the wind direction is similar. We hence obtain a time series of hourly water level, wind speed, and direction from 1 April 2002 to 14 April 2010 by reducing of 20% the entire time series of wind speed at the Chesapeake Light. 22% of the time series had missing data on either water level or wind conditions. For each site, the time series  $H_i$  and  $T_i$  were reconstructed using Equation (7).

#### 4.3.2. Model Validation

The results were validated using two wave events: Period 1, from 31 January to 5 February 2009 and Period 2, from 1 March to 2 March 2009, using wave data collected in the field and reported in Mariotti *et al.* [29]. The performance of SWAN in reproducing wave height and wave period is evaluated using the Root Mean Square Error and the Model Efficiency. The latter measures the ratio of the model error to variability in observational data, and its performance levels are categorized as: >0.65 excellent; 0.65–0.5 very good; 0.5–0.2 good; <0.2 poor [45]. The performance of SWAN is analogous to the numerical model used in Mariotti *et al.* [29]: the Root Mean Square Error in the wave height is around 10 cm, while the Model Efficiency for the wave height is between -2.1 and 0.4 (Figure 5).

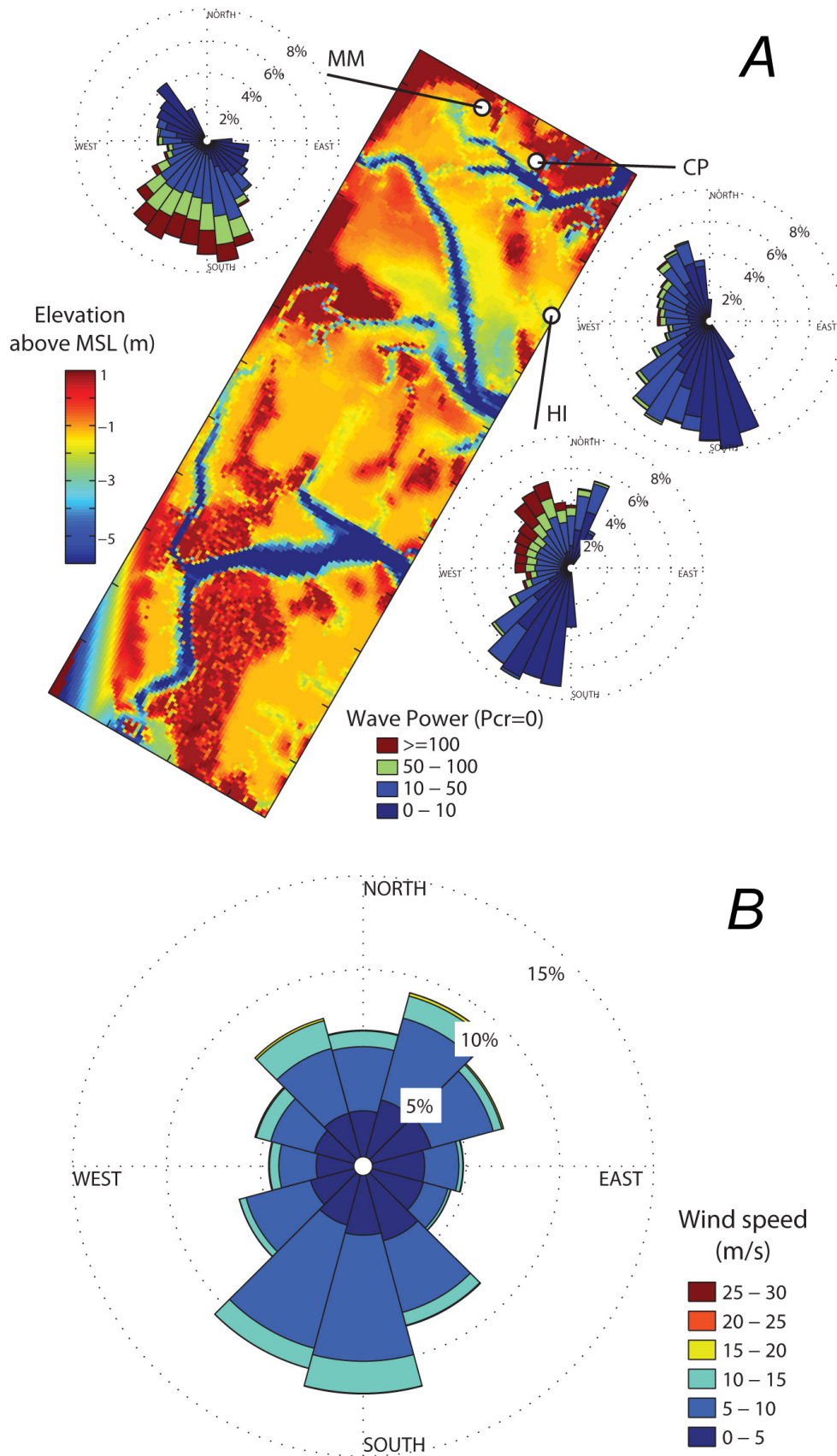


**Figure 4.** (A) Digital elevation model of Hog Island Bay used to hindcast wave height and wave period with the SWAN model. The distribution of wave power (W/m) and directions from the model output is shown for each study location; (B) distribution of wind speed (m/s) and directions used to force the model.

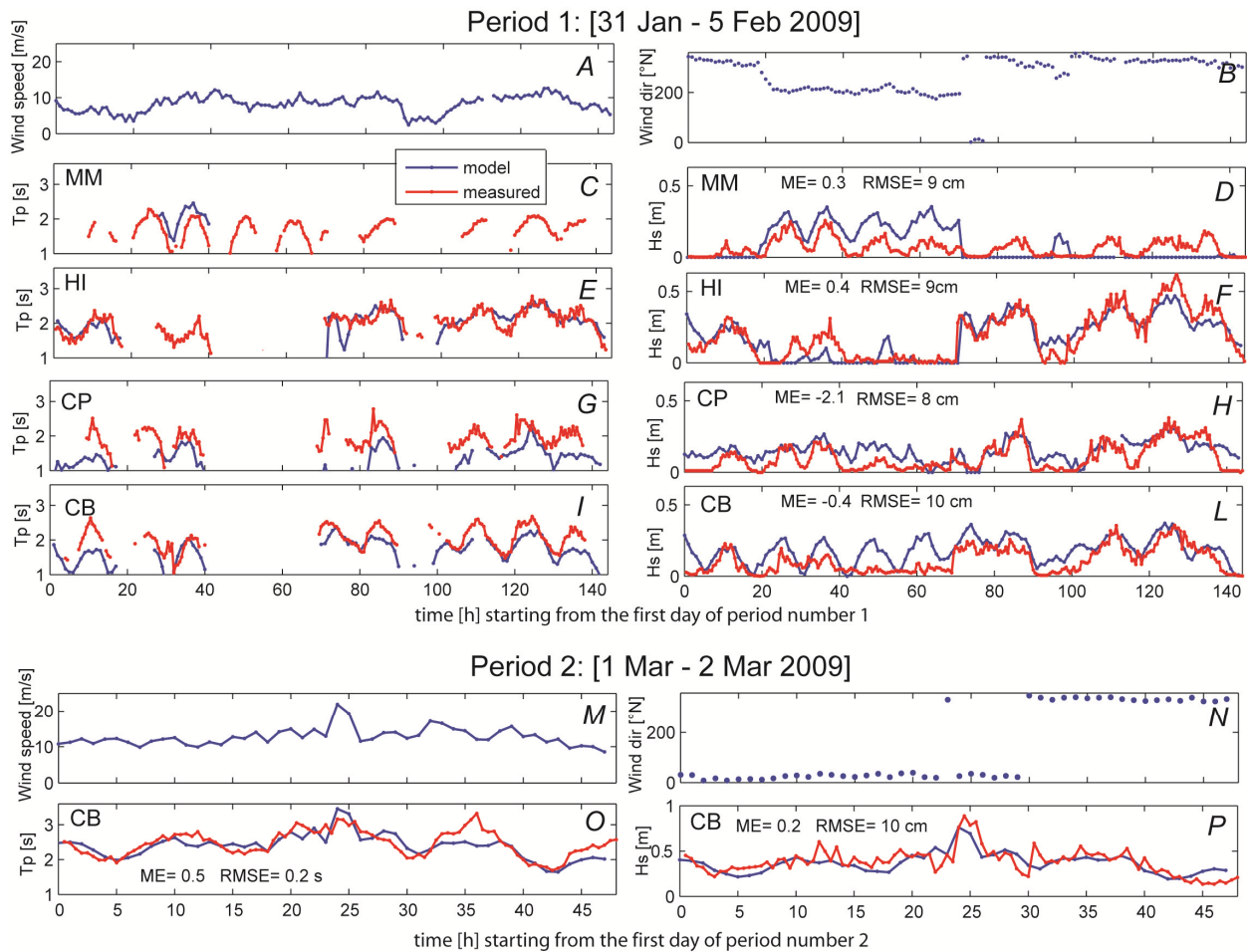


**Figure 5.** Model simulations of significant wave height and wave period validated against measured data for the three study sites. Wind data from NOAA Wachapreague station 8631044; (A) wind speed and (B) wind direction for period 1. Wave period for (C) Matulakin Marsh; (E) Hog Island Marsh; (G) Chimney Pole; (I) Central Bay. Wave height for (D) Matulakin Marsh; (F) Hog Island Marsh; (H) Chimney Pole; (L) Central Bay. (M) wind speed and (N) wind direction for period 2; (O) Wave period for Central Bay; (P) wave height for Central Bay.

#### 4.3.3. Proxy for Salt Marsh Boundary Erosion

Three proxies for marsh boundary erosion were considered: wave height (m) at the marsh boundary, wave power (W/m) incident to the marsh boundary [28] and the wave thrust (kN/m) acting on the marsh boundary [26]. In analogy to erosion of a horizontal bed of sediment (*i.e.*, the Shields parameter), we hypothesize the existence of a threshold in wave energy below which erosion is zero. Wave erosion thresholds were designed to address the effects on erosion due to differences in wave energy magnitude *versus* duration. The goal of this task is to determine whether erosion is predominately a result of low-energy, frequent events, or high-energy infrequent events. We attempt to address this question by computing the wave power using different erosion thresholds and comparing the correlation between results without the threshold.

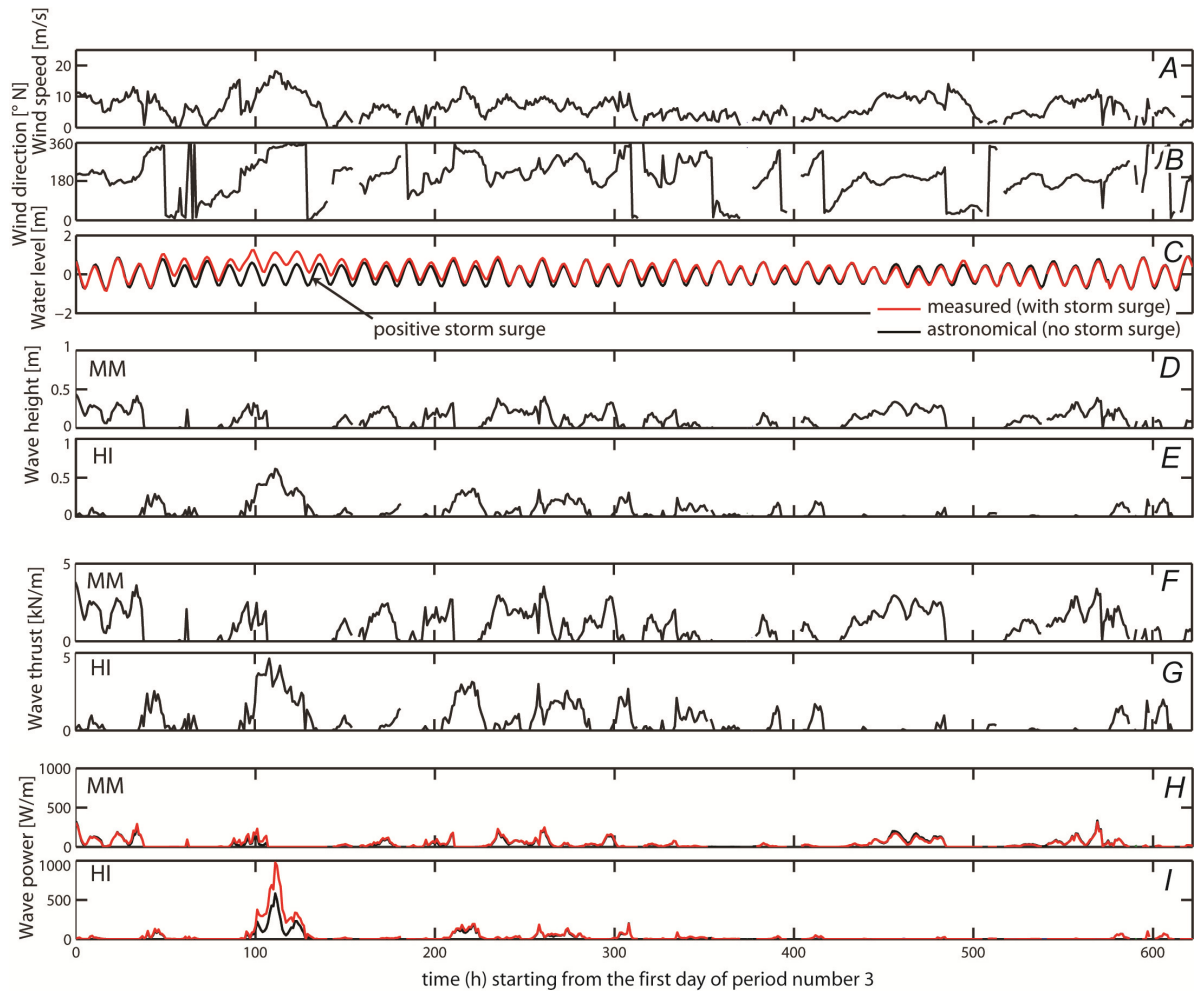


**Figure 6.** Sample time series reconstruction (21 August 2008 to 13 April 2010) of modeled wave height, wave thrust, and wave power using measured (with storm surge) and predicted (no storm surge) water levels for two study sites. The full reconstruction for data analysis spans from 1 April 2002 to 19 April 2010 for all three study sites. Note peak wave power at the HI location ( $t = 110$  h) due to the storm surge, which is double the wave power without storm surge.

The excess incident wave power (W/m) was computed as:

$$P = \begin{cases} c_g E \cos(\theta) - P_{cr} & \text{if } P > P_{cr} \\ 0 & \text{if } P < P_{cr} \end{cases} \quad (8)$$

where  $c_g$  is the group velocity,  $E$  the wave energy ( $J/m^2$ ), and  $\theta$  the angle between the wave direction and the normal to the marsh boundary.  $P_{cr}$  represents a threshold in marsh boundary erosion [29,30], introduced in analogy with the threshold in bottom sediment erosion.

The wave thrust was computed using the results of Tonelli *et al.* [26]. The maximum wave thrust (kN/m) for the case of a vertical bank is approximated as:

$$W = \begin{cases} 8.8 H & \text{if } h < h_b \\ 8.8 H - 11 (h - h_b) & \text{if } h_b < h < h_b + 0.4 \\ 4.4 H & \text{if } h > h_b + 0.4 \end{cases} \quad (9)$$

where  $h$  is the water depth in front of the marsh boundary and  $h_b$  is the height of the marsh platform. The dependence on the period is neglected. Different from wave power, the use of the wave thrust takes into account the effect of reduced marsh boundary erosion when the water level is higher than the marsh top.

Using the time series  $H_i$ ,  $T_i$  and  $y$ , we reconstructed the times series  $P_i$  and  $W_i$ , using both the measured and the predicted water levels. A sample from the whole time series is given in Figure 6. This example clearly shows the effect of storm surges: the maximum wave power (Figure 6,  $t = 110$  h) at the HI site computed by considering the measured water level is almost double the maximum wave power computed with the predicted (astronomical) water level.

## 5. Results

### 5.1. Boundary Retreat Estimates

Since pin measurements may underestimate erosion (due to few data points and missing pins when a slump occurs) the average between the erosion rates calculated with the field survey and the aerial photographs is taken as the best estimate at each site (Table 1). The shoreline along Matulakin marsh eroded the fastest, with an average erosion rate of 1.91 m/year, followed by Chimney Pole (1.28 m/year) and Hog Island (0.88 m/year). The erosion rates computed with erosion pins exhibit the same trend as the seven year (2002–2009) erosion rates derived from GIS and surveys (2008–2010): Matulakin marsh had the highest retreat rate at 0.74 m/year followed by Chimney Pole (0.71 m/year) and Hog Island (0.32 m/year) (Table 1). The degree of erosion underestimation using erosion pins is fairly consistent. In fact, the ratio between erosion measured via erosion pins to that of boundary surveys is similar for all sites, with values 0.39 for MM, 0.51 for CP, and 0.35 for HI, the interpretation being that the retreat rates may be underestimated by roughly 50%–65% when using erosion pins. McLoughlin *et al.* [7] carried out a similar analysis in Hog Island Bay at the same sites studied herein (Hog Island Marsh, Chimney Pole, Matulakin Marsh) using erosion data computed from aerial photographs spanning 50 years. Their erosion rates (MM 1.6 m/year, CP 1.3 m/year, HI 1 m/year) are very similar to those computed in our two years period. The 33 sites analyzed using aerial photography produced an average erosion rate of  $1.47 \pm 1.03$  m/year with 75 percent of the values distributed between 1.0 and 2.0 m/year; only 12 percent of the data exceeded 2.5 m/year with three values being twice the standard deviation from the mean.

The frequency-magnitude distribution of erosion events was calculated by analyzing field data of marsh shoreline for the three sites. The two fastest eroding sites (MM, and CP), have a frequency-magnitude distribution close to a Gaussian distribution. The frequency-magnitude distribution of erosion events in HI has a longer tail and appears closer to a logarithmic distribution (Figure 7). As the average erosion rate increases, the frequency-magnitude distributions approach a Gaussian distribution. The slowest eroding site (HI) has the longest tail of erosion events.

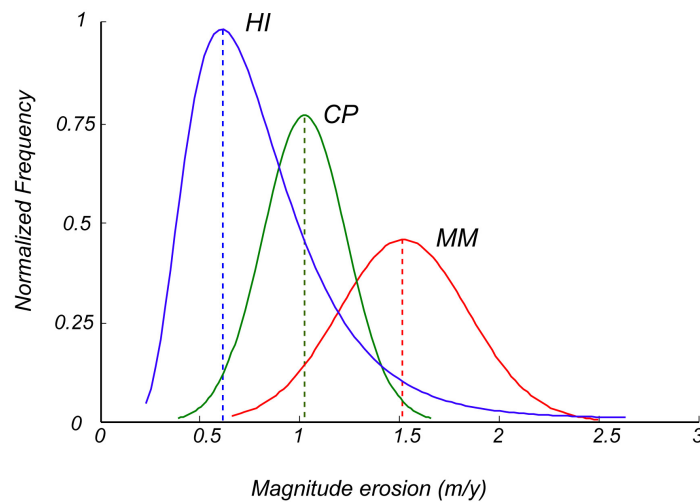


**Figure 7.** Frequency magnitude distribution of erosion events for the three sites where field measurements were collected. Matulakin Marsh (MM); Chimney Pole (CP); Hog Island (HI).

**Table 1.** Erosion at the three study sites estimated from each method (erosion pins, total station surveys, historical imagery). Average of survey and imagery methods is given as a best estimate since erosion pins may underestimate erosion.

Method	Matulakin Marsh			Chimney Pole			Hog Island		
	Cumulative (m)	Duration days	Rate (m/year)	Cumulative (m)	Duration days	Rate (m/year)	Cumulative (m)	Duration days	Rate (m/year)
Pins	1.68	825	0.74	1.87	958	0.71	0.85	958	0.32
Survey	3.71	705	1.92	2.71	705	1.4	1.77	705	0.91
Photos	13.24	2557	1.89	8.18	2557	1.17	5.98	2557	0.85
Average			1.91			1.28			0.88

### 5.2. Erosion as a Function of Shoreline Sinuosity

Sinuosity values for the entire marsh boundary profiles, and thus at the length scale of hundreds of meters, are: 1.18 (in 2008), 1.19 (in 2010) at Chimney Pole; 1.22 (in 2008), 1.21 (in 2010) at Matulakin Marsh; 1.32 (in 2008), 1.30 (in 2010) at Hog Island. Sinuosity values for Chimney Pole, and Matulakin Marsh, which are the two most exposed sites with the highest erosion rates, are similar. Sinuosity values at Hog Island, the most sheltered site are significantly higher (Figure 3).

Apart from Matulakin Marsh, there is a significant correlation between small-scale sinuosity and retreat rates (Figure 8). It is important to notice that this relationship is valid at a relatively small scale (tens of meters), and it is not representative for the entire marsh boundary. Both erosion rates and sinuosity values are locally computed, and are not necessarily reflective of the average across the length of the marsh.

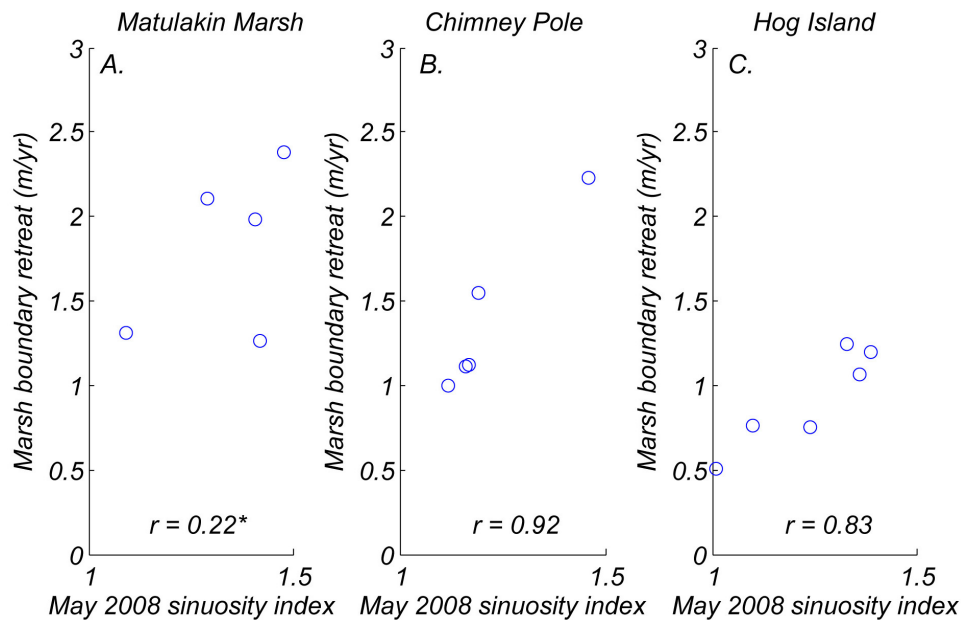


**Figure 8.** Marsh edge erosion rate as a function of shoreline sinuosity. Each data point represents the average erosion rate and sinuosity within each boundary section (see Figure 3) between May 2008 and April 2010. Sinuosity is used as a proxy for the presence of wave-cut gullies, whereby erosion is more vigorous due to concentration of wave energy. These data suggest that a high number of wave gullies resulted in more vigorous erosion. Correlation coefficients ( $r$ ) are also shown and are significant at the 95% confidence level ( $p < 0.05$ ) with the exception of MM.

### 5.3. Retreat as a Function of Wave Power

The investigation of the relationship between wave energy and marsh erosion was analyzed as a function of average wave power and total work done (power  $\times$  time) in each measurement sub-period. First, we examined the site-specific cumulative boundary erosion obtained by erosion pins as a function of the total work done (MJ/m) on the boundary within each of the measurement sub-periods (Figure 9). Predictably, the greater the amount of cumulative wave energy at each site resulted in a greater cumulative retreat of the boundary. However, while larger values of wave energy resulted in greater cumulative erosion, the total amount of erosion measured with pins for a given cumulative wave energy was site specific. For example, HI experienced much less erosion per unit of work done than CP despite being subjected to the greatest total wave energy (Figure 9A).

In addition, we examined cumulative erosion calculated from total station measurements within each sub-period from all three sites as a function of cumulative wave energy (Figure 9B). The total erosion measured with total station surveys follows the same trend of the pin erosion: for a given wave energy, CP erodes the most while HI erodes the least. By converting cumulative erosion and cumulative wave energy in erosion rates and wave power we obtain that for a wave power of 20 W/m the total erosion rates are: HI = 0.51 m/year, MM = 1.10 m/year, CP = 3.82 m/year, while the erosion rates measured by the pins are: HI = 0.23 m/year, MM = 0.47 m/year, CP = 1.07 m/year.

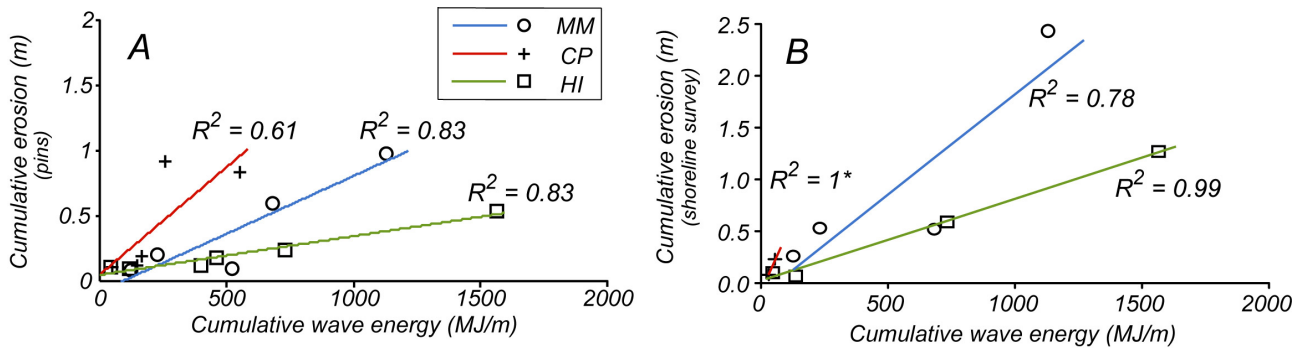


**Figure 9.** (A) Cumulative erosion measured by erosion pins plotted as a function of cumulative wave energy. Greater cumulative wave energy results in greater shoreline retreat; however, the response is site-specific due to inter-site variations in soil properties and marsh elevation; (B) Cumulative erosion (determined from shoreline surveys) plotted as a function of cumulative wave energy. Each data point represents the erosion between four consecutive measurement periods from 8 May 2008 to 13 April 2010. For Chimney Pole only two data points are available.

The erosion rate estimates obtained from GIS analysis at all 33 sites along the bay produce a generalized relationship between erosion rate and average wave power (Figure 10). Despite the large variability in erosion rates, there is a significant relationship ( $R^2 = 0.25$ ,  $p < 0.05$ ) between wave power and erosion rate. If we average the data over regular bins to emphasize the overall trend (black dots in Figure 10A, see also Marani *et al.* [31]) we obtain  $R^2 = 0.66$  ( $p < 0.05$ ) and a linear relationship that reads:  $E = 0.079 P + 0.43$ .

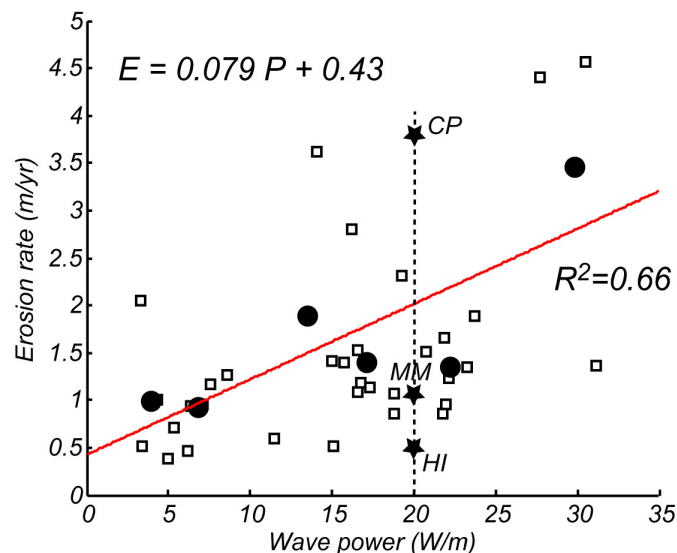


**Figure 10.** Marsh boundary erosion rate derived from GIS shoreline analysis (19 January 2002 to 30 June 2009) as a function of average wave power computed from the SWAN model at 33 sites. Solid black circles indicate values obtained by averaging data over regular “bins” to emphasize the overall trends ( $R^2 = 0.66$  with  $p < 0.05$ ). The three stars represent the erosion data computed from the short-term field measurements with a wave power of 20 W/m.

*5.4. Retreat as a Function of Wave Erosion Thresholds, Wave Height, and Water Level*

To explore the possible presence of a threshold in wave power below which the erosion rate is negligible, we performed several experiments using a prescribed wave erosion threshold on the model output. The total wave power includes only the difference between the computed wave power and a prescribed threshold. Therefore, if the wave power of a specific event was below the threshold, the event was discarded altogether. We further test the existence of a threshold in wave thrust and wave height, such that only events with wave height or wave thrust above a specific value would cause salt marsh erosion. For each new dataset, we computed the correlation coefficient between the modified wave variable and the erosion rate using different threshold values for wave power ( $P_{cr}$ ), wave height ( $H_{cr}$ ), and wave thrust ( $T_{cr}$ ). The goal is to determine what wave variable and threshold value yields the highest correlation coefficient. The results are provided in Table 2. The highest correlation coefficients were obtained with wave power. The correlation coefficient increases when a threshold value is added in the analysis. However, the increase is very subtle and may not be entirely meaningful.

In a second set of analyses we removed the effect of storm surges by utilizing in the calculation of wave climate the astronomic tidal elevation computed by the local harmonic constants, rather than actual water-level measurements. In this way we can single out the effect of storm surges on marsh erosion. The resulting correlation coefficients are higher than values computed by taking into account storm-surges, and follow a similar trend. Without storm surge, correlation coefficients are higher when the erosion is plotted against wave power, and the highest correlation is achieved when a threshold of 50 W/m is considered.

**Table 2.** Summary of correlation coefficients to show the strength between GIS-derived erosion rates and thresholds in the wave variable (meaning values below the threshold are discarded from the computation; see Equations 2) with and without the effects of storm surge.

	Wave Power			Wave Height			Wave Thrust		
	Pcr (W/m)			Hcr (m)			Wcr (kN/m)		
No Storm Surge	0	10	50	0	0.1	0.2	0	0.1	0.2
Correlation R <sup>2</sup> (N = 33)	0.24	0.25	0.28	0.10 *	0.13	0.15	0.11 *	0.14	0.14
With Storm Surge	0	10	50	1	0.1	0.2	0	0.1	0.2
Correlation R <sup>2</sup> (N = 33)	0.22	0.23	0.24	0.11 *	0.12	0.11 *	0.10	0.13	0.11 *

\* Indicates values that are not statistically significant.

**6. Discussion**

*6.1. Variability in Erosion Rates*

Present retreat rates of marsh edges in this study area are commonly on the order of 1 m/year. The high degree of erosion-rate variability for a given wave forcing is most likely due to a combination of factors such as sediment composition, marsh elevation, and the extent of burrowing crabs at each site. For example, research by McLoughlin [46] determined that crab burrow densities at the marsh

edge were about 300% higher at MM ( $200/\text{m}^2$ ), relative to CP and HI ( $\sim 50/\text{m}^2$ ). More notably, however, was that the burrow volumes at CP and MM ( $\sim 11,000 \text{ cm}^3/\text{m}^2$ , and  $8000 \text{ cm}^3/\text{m}^2$ , respectively) were more than ten times greater than at HI ( $\sim 500 \text{ cm}^3/\text{m}^2$ ). Greater burrow densities and volumes may act to enhance erosion under wave impact due to hydraulic action within the pore spaces, especially given the reduced material strength resulting from the cavities.

The erosion rates measured with pins represent the amount of material that is slowly removed on the marsh scarp surface by waves and currents (corrasion), that is, the action of hydraulic pressure on the scarp with or without sediment entrainment. Here, the material is detached in small quantities from each wave impact but can amount to considerable sums over the span of a few months. Erosion pins, however, are unable to capture the detaching of large blocks, scarp slumping, undercutting, or other mass wasting processes (Figure 1D). Comparing the erosion rate from pins against the total erosion rate from the boundary surveys may help elucidate the relative role of corrasion *versus* mass wasting with respect to the total scarp retreat. If this simple analysis reflects reality, then the effect of corrasion is similar at MM and HI (39% and 35%, respectively), and higher at CP (51%). These results suggest that mass wasting processes are important, perhaps accounting for 50%–70% of the total marsh boundary retreat at our sites.

We found a very robust relationship between cumulative erosion and cumulative wave energy, however this relationship considerably varies from site to site (Figure 9). For a given wave energy impacting the marsh boundary in a given period of time, CP erodes the most while HI erodes the least, both in terms of total erosion (*i.e.*, measured with marsh boundary surveys) and corrasion (*i.e.*, measured with erosion pins). This different behavior can be explained by the low volumes of burrows measured at HI. With less crab bioturbation, the soil of the marsh bank is more compact and difficult to erode.

When transformed in wave power and erosion rates, short-term data are consistent to long-term data (Figure 10). Marsh elevation may also have significant control on erosion rates since it controls for how long a marsh cliff may be exposed to waves and tides, and therefore, the total amount of wave power acting on the cliff. Modeling efforts by Tonelli *et al.* [26] showed that maximum wave thrust ( $\text{kN/m}$ ) occurs when the water elevation equals the elevation of the marsh platform. Tidal elevations higher than the marsh platform resulted in a rapid decrease of wave thrust, suggesting that marsh boundaries are protected from waves when drowned. This may explain why HI has the lowest erosion rates since its elevation above mean sea level is 10 cm below that of UN and 20 cm below CP [46]. However, it must also be noted that Hog Island's shoreline orientation is somewhat protected from the strongest dominant winds, which are from the N-NE in winter and SSE-SSW in the summer.

The equivalence between the erosion rates measured in this study in a two years period with those measured by McLoughlin *et al.* [7] in a 50 years period is quite surprising. This indicates that these marshes have been eroding over the past 50 years at the same rate, and that erosion rates are stable across different temporal scales, ranging from months to decades. This is further corroborated by the strong correlations between cumulative erosion and cumulative wave energy at each site (Figure 9). Again this study performed at the monthly scale well agrees with McLoughlin *et al.* [7], who report high coefficient of correlations for the linear regression of total erosion at each site in a 50 years timespan.

Whereas local erosion rates are very stable in time and are related to the temporal evolution of wave energy at a given site, it seems more difficult to connect spatial variations in erosion rates to the spatial distribution of wave energy in the bay. Both our results and McLoughlin *et al.* [7] results display either

a weak correlation (Figure 10) or absence of correlation between wave power and erosion rates. This indicates that local marsh resistance and local mass wasting processes play a major role in marsh erosion. McLoughlin *et al.* [7] indicate that erosion rates corrected by marsh elevation (*i.e.*, the volumetric erosion rates of (Equation (4)) better relate to wave power. Here we further explore the effect of thresholds on wave power, without finding a noteworthy improvement. We also determine that wave power is better suited to represent marsh erosion with respect to wave thrust or wave height. Neglecting storm surges does not decrease the correlation between erosion and wave power. This surprising result is possibly due to the sum of two distinct processes. Higher water levels driven by a storm surge favor the formation of large waves. On the other hand, higher water levels reduce the wave impact on the marsh boundary, as indicated by Tonelli *et al.* [26], because waves rather than breaking at the marsh scarp propagate on the marsh platform where they are dissipated by the vegetation. As a result the bulk of wave energy is no longer released at the marsh boundary. This was also confirmed in laboratory tests, showing that the most critical condition for marsh bank instability is associated to low water levels in front of the bank [47]. These two opposite effects might cancel out reducing the overall importance of storm surges.

## 6.2. Shoreline Sinuosity

An analysis of shoreline sinuosity as a function of marsh retreat revealed that, at the scale of the entire marsh boundary (hundreds of meters), sinuosity values are higher when the marsh boundary is eroding slowly. In fact, the marsh boundary at HI has significantly higher sinuosity than the two more rapidly eroding sites (CP and MM) (Figure 8). The frequency-magnitude distribution of erosion events at HI has a longer tail than the frequency-magnitude distribution for the other two sites. This is in agreement with the presence of a rougher marsh boundary. In fact, despite of the mean of the erosion events being lower, there are a few points in HI that erode at the same rate of the two most exposed sites (Figure 7, blue line; the long tail encompasses values on the horizontal axis of the same order of magnitude of the other two frequency magnitude distributions). For the two most exposed sites, frequency magnitude distributions appear closer to a Gaussian distribution. These results are in agreement with the findings of Leonardi and Fagherazzi [5,6], and have been related to the presence of variability in erosional resistance along the marsh boundary. In fact, the presence of a local variability in erosional resistance leads to a cascade of failures contributing to the generation of rough marsh boundary profiles and long-tailed distribution of the erosion events.

To only focus on the relationship between sinuosity and wave energy, and to exclude from the analysis the influence of variability in soil resistance along the marsh boundary, we further calculated sinuosity values at a smaller scale (tens of meters). At this scale we find that erosion rates increase with sinuosity. We relate this increase in erosion rates to the formation of wave-cut gullies, which are sub-triangular incisions whose erosion has been often found to be three to five times greater than that at the shoreline. This is due to the fact that the action of wind waves is augmented within the gully due to wave reflection and wave-energy concentrations within a gradually smaller cross-sectional area [27]. Small-scale sinuosity and erosion values in Figure 8 are localized phenomena and are not representative of the entire marsh boundary profiles. Therefore, at a small scale, for which erosional resistance is expected to be relatively uniform, the evolution of the marsh scarp is affected by positive feedbacks

between wave action and the morphology of the boundary and these positive feedbacks can lead to a localized increase in marsh boundary sinuosity and erosion. However, at a larger scale where variability in erosional resistance is expected to be present, the more rapidly the marsh erodes the smoother the marsh boundary.

### 6.3. Future Marsh Survival and Sediment Fate

Knowlton [48] reported a net 16% marsh loss within Hog Island Bay over a 116-year period (1852–1968). Erosion rates at the marsh boundary over the past 50 years are similar to modern rates [7], and their average is on the order of 1.3 m/year. This implies that the marsh boundary will retreat another 65 m over the next half century, and may therefore completely vanish over the next half millennia. Considering the predominately eroding perimeter of the marshes to be approximately 28,000 m with an average marsh platform thickness of 1.3 m, then the volume of sediment released to Hog Island Bay is estimated to be on the order of 50,000 m<sup>3</sup>/year, assuming an average erosion rate of 1.3 m/year. Given the average bulk density of marsh sediments in this area to be 0.78 g/cm<sup>3</sup> [46], this translates to approximately 39,000 tons/year of eroded material. The fate of eroded sediments from the marsh edge is varied and may depend on sediment size. Some sediment eroded from the edge is reworked and deposited on the marsh platform some 10–20 m adjacent to the boundary, increasing the platform elevation about 20 cm relative to the interior. Similarly, sediments are typically deposited within a relatively short distance adjacent to marsh creeks, which explains the lower elevations and higher organic content of the marsh interiors compared to the higher elevations along creek banks and marsh boundaries, where sediments typically have less organic content [46,48]. Long-term sedimentation rates in the bay were reported by Ortel *et al.* [49] to be 2.3–3.5 mm/year based on Pb-210 dating of two cores (though these rates do not necessarily reflect a constant upward filling), while sedimentation rates on the marsh platforms were estimated between 1.2 and 1.8 mm/year [50], suggesting that the sediments eroded from the marsh edge are the primary source of sediments to the bay. Similar processes occur in Chincoteague Bay, Virginia, where an estimated 46% of sediment delivery to its bay was sourced from edge erosion [51]. Likewise, cannibalization of the marsh edge is likely the primary source of sediments to the marsh platform [52].

## 7. Conclusions

High-resolution measurements of lateral salt marsh erosion at the sub-meter scale were conducted along the boundary between marshes and Hog Island Bay at the Virginia Coast Reserve, USA. These measurements, together with erosion rates estimated from aerial photographs for a seven years period, complemented and expanded a long-term dataset of marsh erosion at this location [7]. Erosion rates were compared to wind wave characteristics computed with the numerical model SWAN. We confirm the existence of a previously shown relationship between salt-marsh lateral retreat and wave forcing. According to our analysis, salt-marsh erosion is a process continuous in time. This is confirmed by the existence of significant relationships between cumulative wave energy and erosion over sub-periods, as well as between the averages of the same variables.

Salt-marsh boundary erosion is primarily a linear function of wave power, the rate of which averages about 1.3 m/year within Hog Island Bay, Virginia, USA. The primary mechanisms of marsh

retreat are corrasion, block detachment, root-scalping, and formation of wave-gullies, which greatly depend on the tidal elevation during wave generation. At a given site, short-term erosion data (temporal scale of months) are very similar to medium-term erosion data (temporal scale of years) and to the long-term data (temporal scale of decades) reported in McLoughlin *et al.* [7]. However, erosion rates and their relationship to wave power considerably vary from site to site, possibly due to local morphological, sedimentological, and biological factors affecting the resistance of the marsh boundary. At the scale of tens of meters, we found a positive correlation between sinuosity and erosion rate due to positive feedbacks between the morphology of the marsh boundary and wave action, indicative of the formation of wave-cut gullies. However, at a larger scale this relationship is reversed and high sinuosity corresponds to slowly eroding salt marshes, while low sinuosity corresponds to rapidly eroding boundaries.

Marsh erosion is correlated to wave power and less related to wave height or wave thrust. The introduction of a threshold for wave power below which erosion is negligible does not increase in a significant way the correlation between wave power and erosion rate. Similarly, neglecting storm surges does not decrease the correlation between wave power and erosion rate. We therefore conclude that, at the level of approximation of our study, the inclusion in numerical models of a wave power threshold for erosion or the utilization of astronomic tidal elevations rather than measured water levels do not significantly affect the estimate of marsh erosion.

### Acknowledgments

This research was supported by the U.S. Department of Energy's Office of Science (BER) through the Coastal Center of the National Institute for Climatic Change Research at Tulane University award TUL-538-06/07 and by the NSF awards DEB-0621014 (VCR-LTER program).

### Author Contributions

Conceived and designed the experiments: SF AMP GM. Performed the experiments: AMP GM. Analyzed and checked data: AMP GM. Wrote the paper: SF AMP GM NL.

### Conflicts of Interest

The authors declare no conflict of interest.

### References

1. Zedler, J.B.; Kercher S. WETLAND RESOURCES: Status, Trends, Ecosystem Services, and Restorability. *Annu. Rev. Environ. Resour.* **2005**, *30*, 39–74, doi:10.1146/annurev.energy.30.050504.144248.
2. Chen, Q.; Zhao, H. Theoretical Models for Wave Energy Dissipation Caused by Vegetation. *J. Eng. Mech.* **2011**, *138*, 221–229, doi:10.1061/(ASCE)EM.1943-7889.0000318.
3. Fagherazzi, S. Coastal processes: Storm-proofing with marshes. *Nat. Geosci.* **2014**, *7*, 701–702.
4. Mariotti, G.; Fagherazzi, S. Critical width of tidal flats triggers marsh collapse in the absence of sea-level rise. *Proc. Natl. Acad. Sci. USA* **2013**, *110*, 5353–5356, doi:10.1073/pnas.1219600110.

5. Leonardi, N.; Fagherazzi, S. How waves shape salt marshes. *Geology* **2014**, *42*, 887–890, doi:10.1130/G35751.1.
6. Leonardi, N.; Fagherazzi, S. Local variability in erosional resistance affects large scale morphodynamic response of salt marshes to wind waves. *Geophys. Res. Lett.* **2015**, *42*, doi:10.1002/2015GL064730.
7. McLoughlin, S.M.; Wiberg, P.L.; Safak, I.; McGlathery, K.J. Rates and forcing of marsh edge erosion in a shallow coastal bay. *Estuaries Coasts* **2015**, *38*, 620–638, doi:10.1007/s12237-014-9841-2.
8. Fagherazzi, S.; Wiberg, P.L. Importance of wind conditions, fetch, and water levels on wave-generated shear stresses in shallow intertidal basins. *J. Geophys. Res. Earth Surf.* **2009**, *114*, doi:10.1029/2008JF001139.
9. Morris, J.T.; Sundareshwar, P.V.; Nietch, C.T.; Kjerfve, B.; Cahoon, D.R. Responses of coastal wetlands to rising sea level. *Ecology* **2002**, *10*, 2869–2877.
10. Fagherazzi, S.; Kirwan, M.L.; Mudd, S.M.; Guntenspergen, G.R.; Temmerman, S.; D'Alpaos, A.; van de Koppel, J.; Rybczyk, J.M.; Reyes, E.; Craft, C.; *et al.* Numerical Models of Salt Marsh Evolution: Ecological and Climatic Factors. *Rev. Geophys.* **2012**, *50*, doi:10.1029/2011RG000359.
11. Fagherazzi, S. The ephemeral life of a salt marsh. *Geology* **2013**, *41*, 943–944, doi:10.1130/focus082013.1.
12. Fagherazzi, S.; Mariotti, G.; Wiberg, P.L.; MacGlathery, K.M. Marsh collapse does not require sea-level rise. *Oceanography* **2013**, *26*, 70–77.
13. Yapp, R.H.; Johns, D. The salt marshes of the Dovey Estuary. Part II. The salt marshes. *J. Ecol.* **1917**, *5*, 65–103.
14. Redfield, A.C.; Rubin, M. The age of salt marsh peat and its relation to recent changes in sea level at Barnstable, Massachusetts. *Proc. Natl. Acad. Sci. USA* **1962**, *48*, 1728–1735.
15. Hall, S.L.; Wilder, W.R.; Fisher, F.M. An Analysis of Shoreline Erosion along the Northern Coast of East Galveston Bay, Texas. *J. Coast. Res.* **1986**, *2*, 173–179.
16. Philips, J.D. Coastal submergence and marsh fringe erosion. *J. Coast. Res.* **1986**, *2*, 427–436.
17. Finkelstein, K.; Hardaway, S.C. Sedimentation and erosion of estuarine fringing marshes, York River, Virginia. *J. Coast. Res.* **1988**, *4*, 447–456.
18. Allen, J.R.L. Evolution of salt-marsh cliffs in muddy and sandy systems: a qualitative comparison of British west-coast estuaries. *Earth Surf. Process. Landf.* **1989**, *14*, 85–92.
19. Allen, J.R.L. Morphodynamics of Holocene salt marshes: a review sketch from the Atlantic and southern North Sea coasts of Europe. *Quat. Sci. Rev.* **2000**, *19*, 1155–1231.
20. Coops, H.; Geilen, N.; Verheij, H.; Boeters, R.; van der Velde, G. Interactions between waves, bank erosion, and emergent vegetation: An experimental study in a wave tank. *Aquat. Bot.* **1996**, *53*, 187–198.
21. Wilson, C.A.; Allison, M.A. An equilibrium profile model for retreating marsh shorelines in southeast Louisiana. *Estuar. Coast. Shelf Sci.* **2008**, *80*, 483–494, doi:10.1016/j.ecss.2008.09.004.
22. Feagin, R.A.; Lozada-Bernard, S.M.; Ravens, T.M.; Möller, I.; Yeager, K.M.; Baird, A.H. Does vegetation prevent wave erosion of salt marsh edges? *Proc. Natl. Acad. Sci.* **2009**, *106*, 10109–10113.
23. Holdredge, C.; Bertness, M.D.; Altieri, A.H. Role of Crab Herbivory in Die-Off of New England Salt Marshes. *Conserv. Biol.* **2009**, *23*, 672–679.

24. Escapa, M.; Minkoff, D.R.; Perillo, G.M.; Iribarne, O. Direct and indirect effects of burrowing crab *Chasmagnathus granulatus* activities on erosion of southwest Atlantic Sarcocornia-dominated marshes. *Limnol. Oceanogr.* **2007**, *52*, 2340–2349.
25. Davidson, T.M.; De Rivera, C.E. Accelerated erosion of saltmarshes infested by the non-native burrowing crustacean *Sphaeroma quoianum*. *Mar. Ecol. Prog. Ser.* **2010**, *419*, 129–136.
26. Tonelli, M.; Fagherazzi, S.; Petti, M. Modeling wave impact on salt marsh boundaries. *J. Geophys. Res.* **2010**, *115*, C09028, doi:10.1029/2009JC006026.
27. Priestas, A.M.; Fagherazzi, S. Morphology and hydrodynamics of wave-cut gullies. *Geomorphology* **2011**, *131*, 1–13.
28. Schwimmer, R.A. Rate and processes of marsh shoreline erosion in Rehoboth Bay, Delaware, USA. *J. Coast. Res.* **2001**, *17*, 672–683.
29. Mariotti, G.; Fagherazzi, S.; Wiberg, P.L.; McGlathery, K.J.; Carniello, L.; Defina, A. Influence of storm surges and sea level on shallow tidal basin erosive processes. *J. Geophys. Res.: Oceans* **2010**, *115*, doi:10.1029/2009JC005892.
30. Mariotti, G.; Fagherazzi, S. A numerical model for the coupled long-term evolution of salt marshes and tidal flats. *J. Geophys. Res.: Earth Surf.* **2010**, *115*, F01004, doi:10.1029/2009JF001326.
31. Marani, M.; D’Alpaos, A.; Lanzoni, S.; Santalucia, M. Understanding and predicting wave erosion of marsh edges. *Geophys. Res. Lett.* **2011**, *38*, L21401, doi:10.1029/2011GL048995.
32. Terzaghi, K. *Soil Mechanics in Engineering Practice*; John Wiley & Sons: New York, NY, USA, 1996; p. 566.
33. Oertel, G.F. Hypsographic, hydro-hypsographic and hydrological analysis of coastal bay environments, Great Machipongo Bay, Virginia. *J. Coast. Res.* **2001**, *17*, 775–783.
34. Davis, R.E.; Dolan, R. Nor’easters. *Am. Sci.* **1993**, *81*, 428–439.
35. Dolan, R.E.; Lins, H.; Hayden, B. Mid-Atlantic coastal storms. *J. Coast. Res.* **1988**, *4*, 417–433.
36. Hayden, B.P. Climate change and extratropical storminess in the United States: An assessment. *J. Am. Water Resour. Assoc.* **1999**, *35*, 1387–1397.
37. Holthuijsen, L.H.; Booij, N.; Herbers, T.H.C. A prediction model for stationary, short-crested waves in shallow water with ambient currents. *Coast. Eng.* **1989**, *13*, 23–54.
38. Booij, N.; Ris, R.C.; Holthuijsen, L.H. A third-generation wave model for coastal regions: 1. Model description and validation. *J. Geophys. Res.* **1999**, *104*, 7649–7666, doi:10.1029/98JC02622.
39. Ris, R.C.; Holthuijsen, L.H.; Booij, N. A third-generation wave model for coastal regions: 2. Verification. *J. Geophys. Res.* **1999**, *104*, 7667–7681.
40. Yan, L. *An Improved Wind Input Source Term for Third Generation Ocean Wave Modelling*; Koninklijk Nederlands Meteorologisch Instituut, De Bilt, Netherlands, 1987.
41. Cavaleri, L.; Malanotte-Rizzoli, P.M. Wind wave prediction in shallow water: Theory and applications. *J. Geophys. Res.* **1981**, *86*, 10961–10973.
42. Van der Westhuysen, A.J.; Zijlema, M.; Battjes, J.A. Nonlinear saturation-based whitecapping dissipation in SWAN for deep and shallow water. *Coast. Eng.* **2007**, *54*, 151–170.
43. Van der Westhuysen, A.J. Modeling of depth-induced wave breaking under finite depth wave growth conditions. *J. Geophys. Res.* **2010**, *115*, doi:10.1029/2009JC005433.

44. Lawson, S.E.; Wiberg, P.L.; McGlathery, K.J.; Fugate, D.C. Wind-driven sediment suspension controls light availability in a shallow coastal lagoon. *Estuaries Coasts* **2007**, *30*, 102–112.
45. Allen, J.; Somerfield, P.; Gilbert, F. Quantifying uncertainty in high-resolution coupled hydrodynamic-ecosystem models. *J. Mar. Syst.* **2007**, *64*, 3–14.
46. McLoughlin, S.M. Erosional Processes along Salt Marsh Edges on the Eastern Shore of Virginia. M.S. Thesis, University of Virginia, Charlottesville, VA, USA, 2010.
47. Bondoni, M.; Francalanci, S.; Cappiotti, L.; Solari, L. On salt marshes retreat: Experiments and modeling toppling failures induced by wind waves. *J. Geophys. Res. Earth Surf.* **2014**, *119*, 603–620, doi:10.1002/2013JF002967.
48. Knowlton, S.M. Geomorphological History of Tidal Marshes, Eastern Shore, Virginia, from 1852 to 1966. M.S. Thesis, University of Virginia, Charlottesville, VA, USA, 1996; p. 186.
49. Oertel, G.F.; Wong, G.T.F.; Conway, J.D. Sediment accumulation at a fringe marsh during transgression, Oyster, Virginia. *Estuaries* **1989**, *12*, 18–26.
50. Kastler, J.A.; Wiberg, P.L. Sedimentation and boundary changes of Virginia salt marshes. *Estuar. Coast. Shelf Sci.* **1996**, *42*, 683–700.
51. Bartberger, C.E. Sediment sources and sedimentation rates, Chincoteague Bay, Maryland and Virginia. *J. Sediment. Res.* **1976**, *46*, 326–336.
52. Mariotti, G.; Carr, J. Dual role of salt marsh retreat: Long-term loss and short-term resilience. *Water Resour. Res.* **2014**, *50*, 2963–2974.

© 2015 by the authors; licensee MDPI, Basel, Switzerland. This article is an open access article distributed under the terms and conditions of the Creative Commons Attribution license (<http://creativecommons.org/licenses/by/4.0/>).